Structural properties of additive binary hard-sphere mixtures. II. Asymptotic behavior and structural crossovers

Sławomir Pieprzyk [1,*] Santos B. Yuste [2,†] Andrés Santos [2,‡] Mariano López de Haro [3,§] and Arkadiusz C. Brańka [1,‖]

[1]*Institute of Molecular Physics, Polish Academy of Sciences, M. Smoluchowskiego 17, 60-179 Poznań, Poland*

[2]*Departamento de Física and Instituto de Computación Científica Avanzada (ICCAEx), Universidad de Extremadura, Badajoz E-06006, Spain*

[3]*Instituto de Energías Renovables, Universidad Nacional Autónoma de México (U.N.A.M.), Temixco, Morelos 62580, Mexico*

The structural properties of additive binary hard-sphere mixtures are addressed as a follow-up of a previous paper [S. Pieprzyk *et al.*, Phys. Rev. E **101**, 012117 (2020)]. The so-called rational-function approximation method and an approach combining accurate molecular dynamics simulation data, the pole structure representation of the total correlation functions, and the Ornstein-Zernike equation are considered. The density, composition, and size-ratio dependencies of the leading poles of the Fourier transforms of the total correlation functions $h_{ij}(r)$ of such mixtures are presented, those poles accounting for the asymptotic decay of $h_{ij}(r)$ for large r. Structural crossovers, in which the asymptotic wavelength of the oscillations of the total correlation functions changes discontinuously, are investigated. The behavior of the structural crossover lines as the size ratio and densities of the two species are changed is also discussed.

I. INTRODUCTION

The close connection between the thermodynamic properties and the structural correlation functions of fluids in the statistical-mechanical formulation of liquid state theory is well known. In particular, for a fluid mixture of N_c components, the virial route to the equation of state leads to [1–3]

$$Z \equiv \frac{p}{\rho k_B T} = 1 - \frac{\rho}{6 k_B T} \sum_{i,j=1}^{N_c} x_i x_j \int d\mathbf{r} \, g_{ij}(r) r \frac{\partial \phi_{ij}(r)}{\partial r}, \quad (1)$$

where Z is the compressibility factor, p is the pressure, ρ is the number density, k_B is the Boltzmann constant, T is the absolute temperature, x_i is the mole fraction of molecules of species i, $\phi_{ij}(r)$ is the interaction potential (assumed to be spherically symmetric and pairwise additive) between a particle of species i and a particle of species j, and $g_{ij}(r)$ is the radial distribution function (RDF), which is a measure of the probability of finding a molecule of species i at a distance r from another molecule of species j. In the case of hard spheres, Eq. (1) reduces to

$$Z = 1 + \frac{2}{3} \pi \rho \sum_{i,j=1}^{N_c} x_i x_j \sigma_{ij} g_{ij}(\sigma_{ij}), \quad (2)$$

where σ_{ij} is the hard-core diameter of the interaction between a sphere of species i and another sphere of species j, and $g_{ij}(\sigma_{ij})$ is the contact value of the RDF.

*slawomir.pieprzyk@ifmpan.poznan.pl

†santos@unex.es; http://www.unex.es/eweb/fisteor/santos/.

‡andres@unex.es; http://www.unex.es/eweb/fisteor/andres/.

§malopez@unam.mx

‖branka@ifmpan.poznan.pl

On the other hand, from the compressibility route to the equation of state one gets the relationship [3]

$$\chi^{-1} \equiv \frac{1}{k_B T} \left(\frac{\partial p}{\partial \rho} \right)_T = \sum_{i,j=1}^{N_c} \sqrt{x_i x_j} [\mathsf{I} + \widehat{\mathsf{h}}(0)]_{ij}^{-1}$$

$$= 1 - \rho \sum_{i,j=1}^{N_c} x_i x_j \widetilde{c}_{ij}(0), \quad (3)$$

where I is the $N_c \times N_c$ identity matrix and the element $\widehat{h}_{ij}(k) \equiv \rho \sqrt{x_i x_j} \widetilde{h}_{ij}(k)$ of the matrix $\widehat{\mathsf{h}}(k)$ is proportional to the Fourier transform

$$\widetilde{h}_{ij}(k) = \int d\mathbf{r} \, e^{-\iota \mathbf{k} \cdot \mathbf{r}} h_{ij}(r) \quad (4)$$

of the total correlation functions $h_{ij}(r) \equiv g_{ij}(r) - 1$, ι being the imaginary unit. Further, in the last equality of Eq. (3), $\widetilde{c}_{ij}(0)$ is the zero wave-number limit of the Fourier transform

$$\widetilde{c}_{ij}(k) = \int d\mathbf{r} \, e^{-\iota \mathbf{k} \cdot \mathbf{r}} c_{ij}(r) \quad (5)$$

of the direct correlation function $c_{ij}(r)$. The latter is defined through the Ornstein-Zernike (OZ) relation, namely,

$$h_{ij}(r_{12}) = c_{ij}(r_{12}) + \rho \sum_{\ell=1}^{N_c} x_\ell \int d\mathbf{r}_3 \, c_{i\ell}(r_{13}) h_{\ell j}(r_{23}), \quad (6a)$$

$$\widetilde{h}_{ij}(k) = \widetilde{c}_{ij}(k) + \rho \sum_{\ell=1}^{N_c} x_\ell \widetilde{c}_{i\ell}(k) \widetilde{h}_{\ell j}(k), \quad (6b)$$

in real and Fourier spaces, respectively.

Apart from this thermodynamic connection, it has been further established that abrupt changes in the structural correlation functions of a fluid may also show up in its phase

behavior. This is the case of the Fisher-Widom line of simple fluids [4–11], which distinguishes between the region where the large-r behavior of the total correlation function shows damped oscillatory decay (typical of dense and/or high-temperature liquids) and the region where the nature of the decay is monotonic (typical of low-density gases, low-temperature liquids, and near-critical fluids). Structural transitions such as the one related to the Fisher-Widom line, including the physics behind them, are clearly of interest but their study is hampered by the lack of exact results for the structural correlation functions and, despite the availability of interesting work on this subject, additional efforts are clearly required, especially in the case of mixtures.

In a previous paper [12], hereafter referred to as paper I, we presented a method (denoted as the WM scheme) allowing us to obtain an accurate representation of the structural correlation functions of additive binary hard-sphere (BHS) mixtures. The WM method successfully combines molecular dynamics (MD) simulation data, residue-theorem analysis, and the OZ relations, additionally taking into account the tail parts of the structural correlation functions, without using any approximate closures. In particular, by considering a mixture with a fixed diameter ratio of 0.648 and a fixed total packing fraction of 0.5 (which was the system analyzed previously theoretically and through experimental data by Statt *et al.* [13]), we confirmed in paper I the presence of structural crossovers in such a mixture and examined the role played in the crossover by the first two poles of the Fourier transforms of the total correlation functions. We also found very good agreement between the results of the new WM method and those obtained from the use of the rational-function approximation (RFA) [3,14–16] to compute analytically the total correlation functions, as well as an improvement of the agreement between the RFA and WM results and the ones derived from experimental data when compared to the analysis performed in Ref. [13].

The aim of the present paper is twofold. On the one hand, to consolidate the RFA approach as a valuable tool to investigate asymptotic behavior and structural crossover issues, by testing such approach against the results of the WM method. On the other hand, to carry out a more thorough analysis of the role of the pole structure of $\widetilde{h}_{ij}(k)$ on the asymptotic behavior of $h_{ij}(r)$ and the structural crossovers in these functions by considering various BHS mixtures.

The paper is organized as follows. The system of interest (BHS mixtures) is briefly described in Sec. II, where also succinct accounts of the RFA approach and of the WM scheme developed in paper I, as well as some details of our MD simulations, are presented. In Sec. III we provide the basics of the analysis of the poles of the total correlation functions, while in Sec. IV we provide the results of our calculations and an illustration of our main findings. The paper closes in Sec. V with some concluding remarks.

II. STRUCTURAL PROPERTIES OF A BINARY HARD-SPHERE MIXTURE

A. System

Let us consider a binary ($N_c = 2$) fluid mixture of "small" (label s) and "big" (label b) hard spheres. The additive hard

core of the interaction between a sphere of species i and a sphere of species j ($i, j = s, b$) is $\sigma_{ij} = \frac{1}{2}(\sigma_i + \sigma_j)$, where the diameter of a sphere of species i is $\sigma_{ii} = \sigma_i$. Let the number density of the mixture be ρ, the mole fraction of species i be $x_i = \rho_i/\rho$ (where $\rho_i = N_i/V$ is the partial number density, N_i and V being the number of particles of species i and the volume of the system, respectively), and let the size ratio be $q = \sigma_s/\sigma_b \leqslant 1$. From these quantities one can define the partial packing fractions $\eta_i = \frac{\pi}{6}\rho_i\sigma_i^3$ and the total packing fraction $\eta = \eta_s + \eta_b = \frac{\pi}{6}\rho\sigma_b^3(x_s q^3 + x_b)$. Note that in this system there are three characteristic separations between particles at contact, namely, the small-small particle separation, $\sigma_s = q\sigma_b$, the small-big particle separation, $\sigma_{sb} = \frac{1}{2}\sigma_b(1 + q)$, and the big-big particle separation, σ_b.

B. The rational-function approximation method

In order to examine the structural properties, we shall now sketch the RFA approach to obtain the structural properties of additive hard-sphere mixtures. The detailed description of such an approach may be found in Refs. [3,14–16]. First, the Laplace transforms of $rg_{ij}(r)$ are introduced:

$$G_{ij}(z) \equiv \int_0^\infty dr\, e^{-zr} rg_{ij}(r). \tag{7}$$

Next, an explicit form for $G_{ij}(z)$ in terms of a free parameter ξ and an $N_c \times N_c$ matrix $\mathsf{L}(z) = \mathsf{L}^{(0)} + \mathsf{L}^{(1)}z + \mathsf{L}^{(2)}z^2$ is proposed. Then, by imposing certain consistency conditions, the elements of the matrices $\mathsf{L}^{(0)}, \mathsf{L}^{(1)}, \mathsf{L}^{(2)}$ are expressed as linear functions of ξ. In particular, $L_{ij}^{(2)} = 2\pi\xi\sigma_{ij}g_{ij}(\sigma_{ij})$.

Interestingly, the simple choice $\xi = 0$, and hence $L_{ij}^{(2)} = 0$, gives the Percus–Yevick (PY) solution [1,17], which is known to yield different equations of state via the virial [Eq. (2)] and compressibility [Eq. (3)] routes. However, by an appropriate determination of $\xi \neq 0$, the RFA can be made thermodynamically consistent and, additionally, allows one to freely choose the contact values $g_{ij}(\sigma_{ij})$. A convenient choice is provided by the popular BGHLL expression proposed independently by Boublík [18], Grundke and Henderson [19], and Lee and Levesque [20].

Clearly, once $G_{ij}(z)$ has been determined, inverse Laplace transformation directly yields $rg_{ij}(r)$ and hence also $h_{ij}(r)$. On the other hand, explicit knowledge of $G_{ij}(z)$ also allows us to determine the Fourier transform $\widetilde{h}_{ij}(k)$ through the relation

$$\widetilde{h}_{ij}(k) = -2\pi \left.\frac{G_{ij}(z) - G_{ij}(-z)}{z}\right|_{z=\iota k}. \tag{8}$$

In the RFA (as well as in the PY approximation), $G_{ij}(z)$ is obtained from the inner product of the matrix $\mathsf{L}(z)$ and the inverse of another related matrix $\mathsf{B}(z)$. Therefore, the Laplace transforms $G_{ij}(z)$ for all the pairs ij share the same poles, namely, the zeros of the determinant $D(z)$ of $\mathsf{B}(z)$. In the particular case of a binary mixture, the functional form of $D(z)$ is

$$D(z) = \mathcal{P}_6^{(0)}(z) + \mathcal{P}_4^{(s)}(z)e^{-\sigma_s z} + \mathcal{P}_4^{(b)}(z)e^{-\sigma_b z} + \mathcal{P}_2^{(sb)}(z)e^{-2\sigma_{sb}z}, \tag{9}$$

where $\mathcal{P}_6^{(0)}(z)$, $\mathcal{P}_4^{(s)}(z)$, $\mathcal{P}_4^{(b)}(z)$, and $\mathcal{P}_2^{(sb)}(z)$ are polynomials of degrees 6, 4, 4, and 2, respectively. In the PY case ($\xi = 0$), the degrees of those polynomials decrease in two units, i.e., $\mathcal{P}_6^{(0)}(z) \to \mathcal{P}_4^{(0)}(z)$, $\mathcal{P}_4^{(s)}(z) \to \mathcal{P}_2^{(s)}(z)$, $\mathcal{P}_4^{(b)}(z) \to \mathcal{P}_2^{(b)}(z)$, and $\mathcal{P}_2^{(sb)}(z) \to$ const. A basic property of $D(z)$ is $D(0) = 0$, which is tied to the physical condition $\lim_{r \to \infty} g_{ij}(r) = 1$.

It should be stressed that perhaps the most valuable asset of the RFA approach is that, apart from ensuring thermodynamic consistency, it leads to explicit analytic expressions for all the structural properties of the BHS mixture [21]. Additionally, the asymptotic long-range behavior of $h_{ij}(r)$ is directly obtained from the roots of Eq. (9).

C. The WM method

The WM method proposed in paper I [12] allows us to obtain the structural properties of additive BHS mixtures by combining accurate MD simulation data, the pole structure representation of the total correlation functions, and the OZ equation.

In the method, a semiempirical approximation for the structural properties of additive BHS mixtures is constructed by considering the following analytic form of $h_{ij}(r)$:

$$
h_{ij}^{WM}(r) = \begin{cases} -1, & 0 < r < \sigma_{ij}, \\ \sum_{n=1}^{W} b_{ij}^{(n)} r^{n-1}, & \sigma_{ij} < r \leqslant r_{ij}^{\min}, \\ \sum_{n=1}^{M} \frac{A_{ij}^{(n)}}{r} e^{-\alpha_n r} \sin\left(\omega_n r + \delta_{ij}^{(n)}\right), & r \geqslant r_{ij}^{\min}. \end{cases}
$$
(10)

The parameters $\{b_{ij}^{(1)}, b_{ij}^{(2)}, \ldots, b_{ij}^{(W)}\}$ and $\{A_{ij}^{(1)}, \alpha_1, \omega_1, \delta_{ij}^{(1)}, \ldots, A_{ij}^{(M)}, \alpha_M, \omega_M, \delta_{ij}^{(M)}\}$ are obtained by enforcing the BGHLL contact values and the continuity conditions at $r = r_{ij}^{\min}$, and by a nonlinear fitting procedure based on the minimization of $|h_{ij}^{WM}(r) - h_{ij}^{\mathrm{MD}}(r)|$ for each $r/\sigma_{ij} \in (1, r_c^*)$, where $h_{ij}^{\mathrm{MD}}(r)$ is obtained from our MD simulations, the details of which will be specified below. In our fitting procedure, the values of $|h_{ij}^{WM}(r) - h_{ij}^{\mathrm{MD}}(r)|$ for $1 < r/\sigma_{ij} < r_c^*$ were required to be smaller than 10^{-3}. The suitable value of r_c^* depends on the size ratio q and we took $r_c^* = 5, 4, 3$, and 3 for $q = 0.648, 0.4, 0.3$, and 0.2, respectively. This value is connected with the half-length of the simulation box. Note that decreasing q causes a decrease of the available space (smaller simulation box). Therefore, in order to carry out simulations and increase the simulation box with the assumed r_c^* values, it was necessary to add more spheres in the cases $q = 0.3$ and 0.2. For our calculations an appropriate choice for $r_{ij}^{\min}$ was the position of the first minimum of $h_{ij}(r)$. Also, as in paper I, for the subsequent calculations we will usually take $W = 15$ and $M = 10$.

D. Details of the molecular dynamics simulations

The computation of $h_{ij}^{\mathrm{MD}}(r)$ was performed with the DynamO program [22] for the size ratios $q = 0.648, 0.4, 0.3$ and 0.2, and different values of the partial packing fractions (η_b, η_s), which were chosen according to the investigated size ratio to examine a substantial part of the phase diagram (in-

TABLE I. BHS mixtures investigated by MD in this work.

q	η_b	η_s
0.648	0.10	0.20, 0.25, 0.30, 0.35, 0.40
	0.20	0.15, 0.20, 0.25, 0.30, 0.35
0.4	0.05	0.05, 0.10, 0.15, 0.20, 0.25, 0.30, 0.35
	0.20	0.05, 0.10, 0.15, 0.20, 0.25
0.3	0.05	0.10, 0.15, 0.20, 0.25, 0.30, 0.35
	0.20	0.10, 0.15, 0.20
0.2	0.02	0.25
	0.20	0.10

cluding low, moderate, and high total densities) of the BHS mixture. More specifically, the values of the partial packing fractions studied by MD are given in Table I and denoted in Fig. 3 as open yellow circles.

In order to reduce sufficiently finite-size effects and the statistical errors in the simulations, the data of $h_{ij}^{\mathrm{MD}}(r)$ for $r/\sigma_{ij} < r_c^*$ must be obtained from long simulations with a large number of particles ($N \sim 10^4$). It has been checked that 16 384 particles were sufficient to obtain reasonably accurate data for the size ratios $q = 0.648$ and 0.4. In the cases $q = 0.3$ and 0.2, due to the reduction of the size of the simulation box, the systems were investigated with 48 668 particles. The histogram grid size of $h_{ij}^{\mathrm{MD}}(r)$ was set to $\delta r/\sigma_{ij} = 0.01$, which was found to be a suitable choice to balance finite-size effects and statistical errors.

The MD simulations were carried out typically for a total number of 2×10^9 collisions, and the statistical uncertainty of $h_{ij}^{\mathrm{MD}}(r)$ was obtained with the block averaging method [23]. For each density, and in the whole range $r/\sigma_{ij} \in (1, r_c^*)$, the accuracy of $h_{ij}^{\mathrm{MD}}(r)$ was such that the estimated uncertainty was typically smaller than 10^{-3}, being up to 0.005 near contact (for the highest densities) and becoming less than 0.0002 at larger particle separations. For large systems, the finite-size effects in the MD calculations of the RDF arise mainly from fixing the particle number, i.e., from the relation between canonical and grand-canonical ensembles. The corrections required to convert data from the MD simulations to the canonical ensemble are of $O(1/N^2)$ [24,25], which are negligible here. Also, it was checked for a few densities that the remaining part of the correction factor involving density derivatives was smaller than the obtained data accuracy and therefore could be neglected.

III. POLE ANALYSIS AND STRUCTURAL CROSSOVER

In general, the representation of the total correlation functions of additive BHS mixtures may be expressed as [2,26–28]

$$
h_{ij}(r) = \begin{cases} -1, & 0 < r < \sigma_{ij}, \\ \sum_{n=1}^{\infty} \frac{A_{ij}^{(n)}}{r} e^{-\alpha_n r} \sin\left(\omega_n r + \delta_{ij}^{(n)}\right), & r > \sigma_{ij}. \end{cases}
$$
(11)

In fact, the functional form of $h_{ij}^{WM}(r)$ for $r > r_{ij}^{\min}$ in Eq. (10) is based on Eq. (11). While the amplitudes, $A_{ij}^{(n)}$, and the phase shifts, $\delta_{ij}^{(n)}$, are specific for each $h_{ij}(r)$, the damping coefficients, α_n, and the oscillation (angular) frequencies, $\omega_n \equiv 2\pi/\lambda_n$ (λ_n being the associated wavelengths),

are common to all the pairs [27]. Although an infinite number of terms is formally considered in Eq. (11), only a few leading terms (those with the smallest damping coefficients) are needed to characterize the asymptotic behavior of $h_{ij}(r)$. Note that, while each ω_n is actually a wave number, we will use throughout this paper the nomenclature "frequency" with the proviso that it does not refer here to time but to space.

A successful way to study the asymptotic decay behavior of the total correlation functions is based on the pole analysis of their Laplace or Fourier transforms. In Laplace space, the real and imaginary parts of the complex poles $z_n = -\alpha_n \pm \iota \omega_n$ provide the damping coefficient and the oscillation frequencies, respectively. Similarly, in Fourier space the poles are $k_n = -\iota z_n = \pm \omega_n + \iota \alpha_n$. In order to avoid later confusion, it is convenient at this stage to clarify the nomenclature we adopt in this work. We will refer to leading, subleading, sub-subleading, etc. poles to an order in increasing α_n, while the nomenclature first, second, third, etc. poles will refer to an increasing order in ω_n. Apart from that, it must be remarked that the infinite set of poles includes roots with $\omega_n = 0$ (thus representing contributions decaying monotonically), although they are generally far from the most dominant ones.

Depending on the values of the parameters of the BHS mixture, the position of the poles in the complex plane varies. In the simplest scenario, given a size ratio q, the plane η_s vs η_b can be split into two main regions such that the leading pole in one of the regions has an angular frequency $\omega \approx 2\pi/\sigma_b$, which corresponds to a wavelength in the oscillatory decay of the total correlation function comparable to the diameter of the big spheres (i.e., $\lambda \approx \sigma_b$), while in the other region the leading pole has $\omega \approx 2\pi/\sigma_s$ (i.e., $\lambda \approx \sigma_s$) [12,26,27]. The line separating both regions signals a *structural crossover* behavior in which the wavelength $\lambda \equiv 2\pi/\omega$ of the oscillations in the large-r asymptotic regime changes discontinuously from approximately σ_b to approximately σ_s as the relative amount of the small spheres is increased. This crossover line in the η_s vs η_b phase diagram occurs when the corresponding two pairs of poles have the same α. As will be seen in Sec. IV, this basic scenario for the structural crossover can become much more complicated as the total packing fraction increases, giving rise to the presence of "harmonics" of the "fundamental" oscillation frequency $1/\sigma_b$.

Further, we will talk about a first-order, a second-order, a third-order, etc. crossover to the one involving a change in the leading, subleading, sub-subleading, etc. pole, respectively. In particular, for different values of q, η_s, and η_b, the decay of $h_{ij}(r)$ is determined by different combinations of poles (i.e., first and second, first and third, first and fifth, and so on).

As said before, in the RFA the poles are obtained from the zeros of $D(z)$ in Eq. (9) and as follows in the case of the WM scheme. Once the total correlation functions $h_{ij}^{WM}(r)$ [see Eq. (10)] are known after fitting the parameters to the MD data, the direct correlation functions $c_{ij}^{WM}(r)$ are determined via Fourier transforms and the OZ relation in Eq. (6b), as described in paper I [12]. This in turn allows one to find the poles by the method of Evans *et al.* [26] [see Eqs. (21) of paper I].

IV. RESULTS

Evidence of the crossover behavior in BHS mixtures was first pointed out by Grodon *et al.* [27,29], who used two

different formulations of Rosenfeld's fundamental measure theory: the original Rosenfeld functional (which is equivalent to the PY approximation) and the White Bear version. Such crossover behavior was later also mentioned in connection with experiments with colloidal suspensions [13,30].

Let us now turn to the RFA predictions. We begin with the analysis of the leading pole in the η_s vs η_b plane. The detailed landscape as one changes the size ratio is rather complex, so here we provide the most general features [31]. By focusing on the behavior of the oscillation frequency ω associated with the leading pole, one can observe that, given a value of q, the η_s vs η_b plane splits into different regions, in each one of which the (reduced) natural frequency $\omega\sigma_b/2\pi \equiv \sigma_b/\lambda$ is of order of 1 (region R_1) or is of order of $n = 2, 3, \ldots$ (region R_n). The most relevant regions are R_1 (where $\lambda \approx \sigma_b$) and R_{n_s} (where n_s is the integer closest to $1/q$, so that $\lambda \approx \sigma_s$). Both regions are separated by a crossover line (hereafter labeled as C), which is present for any q. Interestingly, as q decreases (and thus n_s increases), one can observe a second crossover line (C') separating region R_{n_s} from either region R_{n_s+1} or region R_{n_s-1}, and even a third line (C'') separating region R_1 from region R_{n_s-1}.

The previous scenario can be observed in Fig. 1, which shows the evolution of the different regions and crossover lines as one decreases the size ratio from $q = 0.648$ to $q = 0.250$. At $q = 0.648$ it is quite apparent the existence of the conventional crossover line C separating the regions R_1 (below the line) and $R_{n_s} = R_2$ (above the line). Interestingly, the line C terminates at an "end point," so that one can move continuously between regions R_1 and $R_{n_s} = R_2$ by circumventing the end point from the left. Decreasing the size ratio from $q = 0.648$ to $q = 0.500$ (top row of Fig. 1) produces a downward bending of line C and a left shift of the end point until it eventually disappears at $\eta_b = 0$. Let us now analyze the middle row of Fig. 1. At $q = 0.425$, region $R_{n_s+1} = R_3$ starts to compete with region $R_{n_s} = R_2$, thus giving rise to the second crossover line C', which terminates at a new end point. At the transition value $q = 0.400$ (where n_s could equally be taken as 2 or 3) the preceding line C' has started a tendency to bend down and the end point has moved to the left. Next, at $q = 0.375$, R_3 has changed from being the old region R_{n_s+1} to being the new region R_{n_s}, while R_2 has changed from being the old region R_{n_s} to being the new region R_{n_s-1}. Moreover, the old line C' has merged with line C producing a "splitting point" (where three different pairs of poles share the same damping coefficient α); now, the crossover line C extends to the right of the splitting point, while to the left it experiences a pitchfork bifurcation into a line C' (separating region $R_{n_s} = R_3$ from region $R_{n_s-1} = R_2$ and still having an end point) and a line C'' (separating regions R_1 and $R_{n_s-1} = R_2$). At $q = 0.350$, the splitting point has moved to the left, the end point of line C' has disappeared, and the residual region R_{n_s-1} has significantly shrunk. In the bottom row of Fig. 1, we see that, at $q = 0.315$, region R_2 has almost disappeared, region $R_{n_s+1} = R_4$ starts to compete with region $R_{n_s} = R_3$, and a new line C' with an end point appears, in analogy with what happened at $q = 0.425$. The rest of the evolution is analogous to what has just been described in relation with the middle row: line C' moves down, it eventually merges with line C creating a splitting point, a relay from old region R_{n_s+1} to new
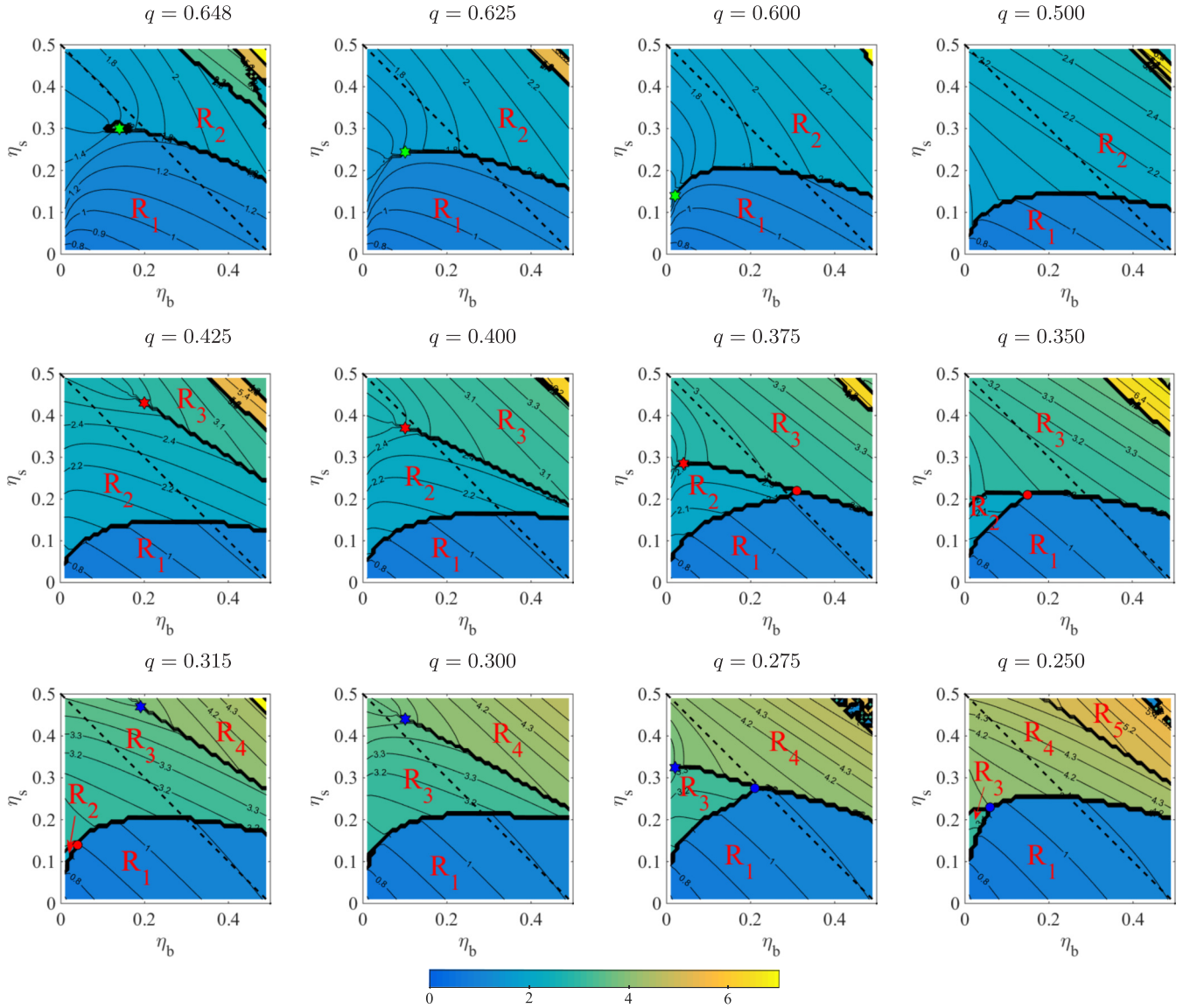
FIG. 1. RFA predictions for the contour plots of the (reduced) oscillation frequency $\omega\sigma_b/2\pi \equiv \sigma_b/\lambda$ corresponding to the leading pole for decreasing representative values of the size ratio (from $q = 0.648$ to $q = 0.250$). The colormap in the bottom bar indicates the color code for the values of $\omega\sigma_b/2\pi$. In each panel, the (black) dashed diagonal line represents the locus $\eta_s + \eta_b = 0.5$. The (colored) stars and circles indicate the end points and the splitting points, respectively. Note that $n_s = 2$ for $q = 0.648, 0.625, 0.600, 0.500$ and 0.425, $n_s = 3$ for $q = 0.375, 0.350, 0.315$, and 0.300, and $n_s = 4$ for $q = 0.275$ and 0.250.

region R_{n_s} and from old region R_{n_s} to new region R_{n_s-1} takes place, and region R_{n_s-1} shrinks until eventually disappearing.

A splitting point is absent in the sequence represented by the top row of Fig. 1. In the second row, however, a splitting point (joining regions R_1, R_2, and R_3) is generated and then it disappears, giving rise to the generation of a new splitting point (joining regions R_1, R_3, and R_4) and its later disappearance along the bottom row. Thus, we will refer to the behavior represented by the top, middle, and bottom rows of Fig. 1 as generations G0, G1, and G2, respectively. As q keeps decreasing beyond $q = 0.250$, a new generation G3 appears. The evolution with q of the end point (generations G0–G3) and splitting points (generations G1–G3) are shown in Fig. 2.

At this stage we should point out two things. On the one hand, it is worth mentioning that the presence of a second

crossover line (i.e., the C' line) was already also reported in Ref. [27], at least for $q = 0.4$. Nevertheless, the distinction between the C, C', and C'' lines that we have made here is important for understanding and/or predicting the structural crossover behavior, including the appearance of different branches for different q systems. For instance, without such assets, neither the reason for the sequence of the crossover lines in Fig. 5 of Ref. [27] nor the reasons for the appearance of the second crossover in the case $q = 0.4$ or of the behavior observed in the case $q = 0.65$ can be explained. In any case, the overall view of the structural crossovers becomes clearer once one realizes that the scenario depicted by Figs. 1 and 2 takes place. Note in particular that, notwithstanding the theoretical interest of the crossover line C', it must be remarked that, as seen from Fig. 1, it generally lies (except
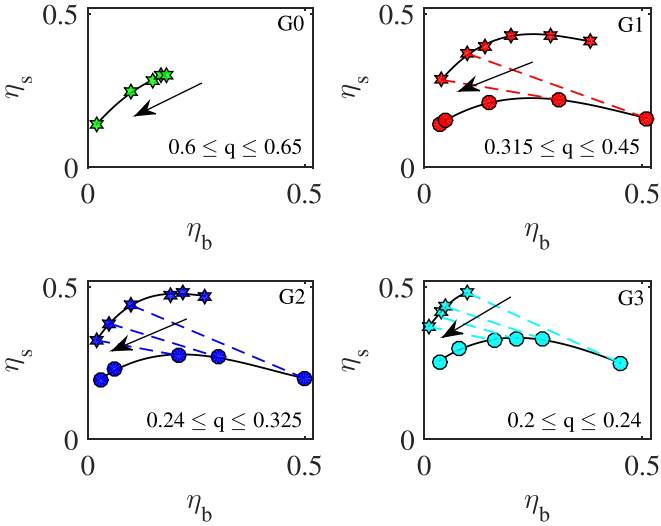
FIG. 2. The q-evolution of the end point (colored stars) and the splitting point (colored circles) of the generations G0–G3. The arrows signal the evolution as q decreases. The dashed tie lines connect end and splitting points at the same q.

for sufficiently asymmetric mixtures) above the region $\eta_s + \eta_b = 0.5$, where the fluid phase is expected to coexist with a solid phase [32]. On the other hand, it should also be clear

that the present scenario is only a coarse-grained description and, while providing a fair picture of what goes on, is not geared towards addressing all the details pertaining to shrinking regions, the merging of crossover lines, the disappearance and appearance of end points, and the formation of splitting points.

To complete the picture advocated in the present paper, let us now present the results of the RFA and the WM scheme for both the damping coefficient and the oscillation frequency associated with the leading pole for $q = 0.2$, 0.3, 0.4, and 0.648. These results are displayed in Fig. 3. We observe that the leading damping coefficient smoothly changes with η_s, η_b, and q, except for the presence of kinks signaling pole crossings. In general, given a value of η_s, the reduced damping coefficient $\alpha\sigma_b$ decreases with increasing η_b. On the other hand, $\alpha\sigma_b$ exhibits a nonmonotonic dependence on η_s at fixed η_b. In what respects q, its influence on $\alpha\sigma_b$ is rather weak, although there is a general tendency for a slight decrease of $\alpha\sigma_b$ with increasing q at fixed (η_b, η_s). In contrast to the behavior of the damping coefficient, the oscillation frequency can experience discontinuous changes in the η_s vs η_b diagram at a given q, as discussed above in connection with Fig. 1. The complexity of the landscape beyond the description of Fig. 1 is exemplified by Fig. 3(e) for $q = 0.2$, where, apart from the pitchfork bifurcation at $(\eta_b, \eta_s) \simeq (0.04, 0.26)$ (giving rise to an encapsulated region R_4), a second splitting point is born at $(\eta_b, \eta_s) \simeq (0.29, 0.38)$.
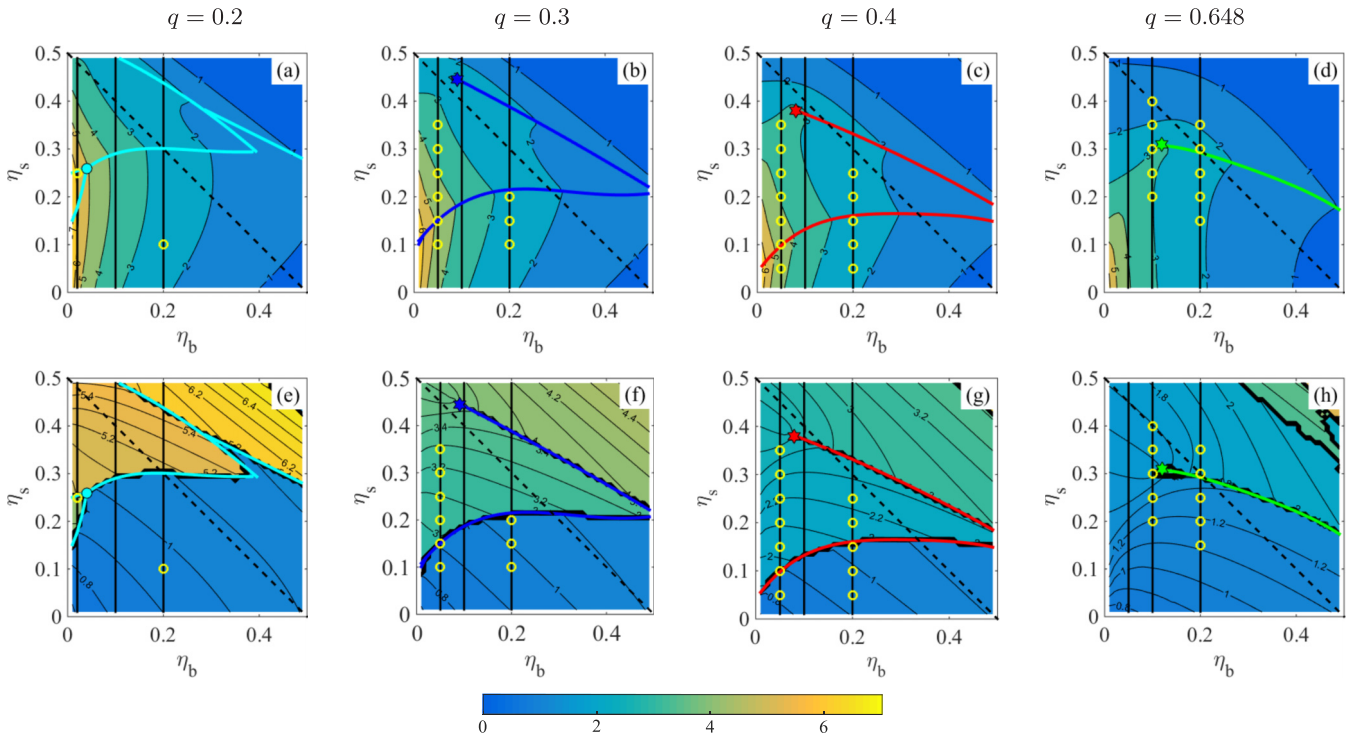

FIG. 3. RFA predictions for the contour plots of the (reduced) damping coefficient $\alpha\sigma_b$ (top panels) and the (reduced) oscillation frequency $\omega\sigma_b/2\pi \equiv \sigma_b/\lambda$ (bottom panels) corresponding to the leading pole for a size ratio (a, e) $q = 0.2$, (b, f) $q = 0.3$, (c, g) $q = 0.4$, and (d, h) $q = 0.648$. The colormap in the bottom bar indicates the color code for the values of $\alpha\sigma_b$ and $\omega\sigma_b/2\pi$. In each panel, the (black) dashed diagonal line represents the locus $\eta_s + \eta_b = 0.5$, the (black) solid vertical lines represent the values $\eta_b = 0.02$ (for $q = 0.2$) or 0.05 (for $q = 0.3$, 0.4, and 0.648), 0.10, and 0.20 considered in Figs. 6–9, and the (yellow) circles denote those cases where MD simulations have been performed. The (colored) thick solid lines represent the crossover lines, while the solid (colored) stars and circles indicate the end points and the splitting points, respectively.
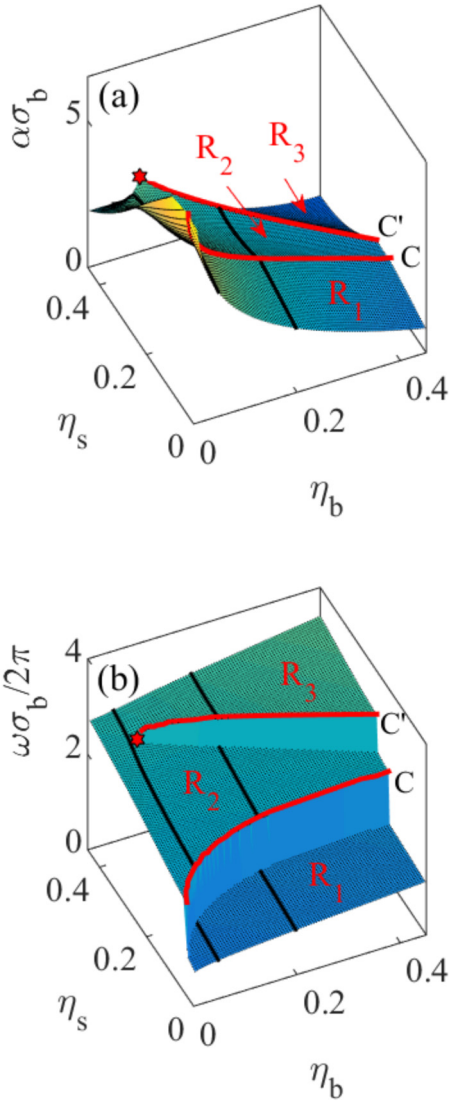
FIG. 5. RFA (thick lines) and PY (thin lines) predictions for the crossover lines C and C' in the plane η_s vs η_b for $q = 0.2$, 0.3, 0.4, and 0.648. The solid circles represent results from MD computer simulations (via the WM scheme), which confirm the theoretical RFA predictions. The WM points for $\eta_b = 0.2$ correspond, from top to bottom, to $q = 0.648$, 0.3, and 0.4, respectively, whereas for $\eta_b = 0.05$ the points correspond to $q = 0.3$ and 0.4. The (magenta) diamond represents a result from paper I [12]. The solid (colored) stars indicate the end points (see Figs. 1–4), while the solid (cyan) circles represent the splitting points of G3 generation (see Figs. 1 and 2). The (black) vertical lines represent the values $\eta_b = 0.02$, 0.05, 0.10, and 0.20 considered in Figs. 6–9.

FIG. 4. 3D plots, as predicted by the RFA, for (a) the (reduced) damping coefficient $\alpha \sigma_b$ and (b) the (reduced) oscillation frequency $\omega \sigma_b / 2\pi \equiv \sigma_b / \lambda$, corresponding to the leading pole for a size ratio $q = 0.4$. The used colormap is the same as the one in Fig. 3; it indicates the change in $\alpha \sigma_b$ in the case of panel (a) and of $\omega \sigma_b / 2\pi$ in the case of panel (b). In each panel, the (black) solid lines represent the cuts $\eta_b = 0.05$ and 0.20 considered in Fig. 8. The (red) thick lines represent the crossover lines and the solid (red) star indicates the end point.

As a representative example, Fig. 4 shows a 3D view visualizing the overall structure behavior, in particular the crossover lines C and C' and the specific regions R_1, R_2, and R_3 for the size ratio $q = 0.4$. This helps the understanding of the different features observed in Figs. 1 and 3, as well as in Figs. 6–9 below. In particular, Fig. 4(b) shows that, as said before, one can move continuously between regions R_2 and R_3 by circumventing the end point.

For the investigated cases $q = 0.2$, 0.3, 0.4, and 0.648, the crossover lines C and C' are plotted in Fig. 5, where RFA and PY predictions, as well as a few points obtained via the WM scheme, are represented. As can be observed, the shape of lines C and C' is qualitatively similar for $q = 0.3$ and $q = 0.4$,
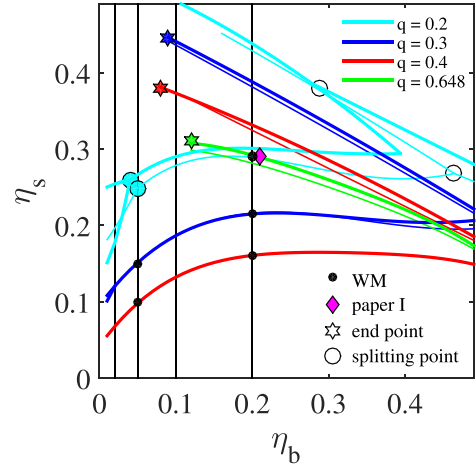
while the cases $q = 0.2$ and $q = 0.648$ present distinctive features. We observe that the black solid circle representing the result from the WM method for $q = 0.648$ and $\eta_b = 0.20$ lies on the line obtained from the RFA prediction better than on the PY line. It is worth noting that the differences between RFA and PY grow with increasing density and decreasing size ratio, being especially apparent for $q = 0.2$. In that case, for instance, the second splitting point changes from $(\eta_b, \eta_s) \simeq (0.29, 0.38)$ in the RFA to $(\eta_b, \eta_s) \simeq (0.46, 0.27)$ in the PY approximation. In any case, it must be remarked that the main separation between the RFA and PY lines for $q = 0.2$ takes place in regions of the plane (η_b, η_s) where the total packing fraction is rather large ($\eta > 0.6$) and hence the stable system is expected to consist of coexisting fluid and solid phases [32].

The information presented in Figs. 3 and 5 is complemented by Figs. 6–9 for $q = 0.2$, 0.3, 0.4, and 0.648, respectively, where the dependence on η_s of the first six poles is shown for $\eta_b = 0.02$ [for $q = 0.2$] or 0.05 [for $q = 0.3$, 0.4, and 0.648] (top panels), 0.10 (middle panels), and 0.20 (bottom panels). It can be observed that typically the first poles correspond to (reduced) frequencies $\sigma_b / \lambda \approx 1$, $\sigma_b / \lambda \approx 1/q$, and the first few harmonics $\sigma_b / \lambda = 2, 3, 4, \ldots$. Note that a certain overlap between the pole with $\sigma_b / \lambda \approx 1/q$ and that with the nearest harmonic might exist, in what could be viewed as sort of "resonance." This happens for $\sigma_b / \lambda \approx 5$, $\sigma_b / \lambda \approx 3$, $\sigma_b / \lambda \approx 2$, and $\sigma_b / \lambda \approx 2$ in the cases $q = 0.2$ (see right panels of Fig. 6), $q = 0.3$ (see right panels of Fig. 7),
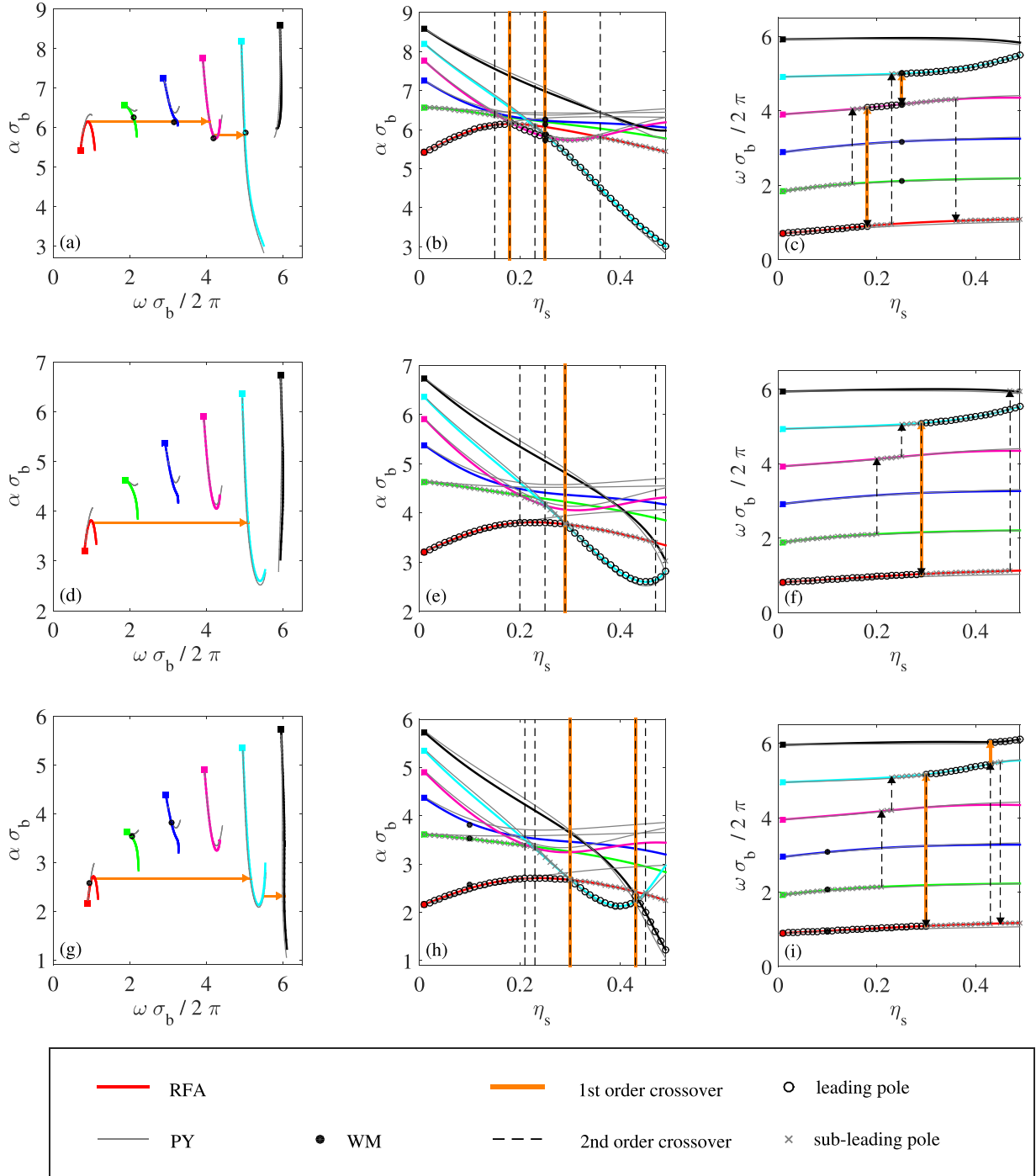
FIG. 6. Dependence of the first six poles on η_s for $q = 0.2$ and $\eta_b = 0.02$ (top panels), $\eta_b = 0.10$ (middle panels), and $\eta_b = 0.20$ (bottom panels). The thick (colored) and thin (gray) lines correspond to the RFA and PY predictions, respectively, while the solid circles represent the WM values for the cases where MD simulations were performed. The colored squares denote poles for a small sphere packing fraction $\eta_s = 0.01$, and the lines indicate trajectories for increasing values of η_s. The horizontal lines denote the crossovers as η_s increases. In the central and right panels, the open circles and crosses represent the leading and subleading poles, respectively.

$q = 0.4$ (see right panels of Fig. 8), and $q = 0.648$ (see right panels of Fig. 9), respectively.

As seen from Figs. 7(c) and 8(c), only the conventional crossover C is present at $\eta_b = 0.05$ for $q = 0.3$ and 0.4, in agreement with what is observed in Figs. 3(f) and 3(g). On the other hand, Figs. 7(f), 7(i), 8(f), and 8(i) show that the crossover C is followed by the crossover C' as η_s increases

at $\eta_b = 0.10$ and 0.20. In the case $q = 0.2$, Fig. 6(c) shows two successive crossovers with $\eta_b = 0.02$ when traversing the two branches stemming from the pitchfork bifurcation at the splitting point $(\eta_b, \eta_s) \simeq (0.04, 0.26)$. Also for $q = 0.2$, the crossovers C and C' are observed in Fig. 6(i) at $\eta_b = 0.20$, while at $\eta = 0.10$ the second crossover C' is beyond the range of η_s shown [see Figs. 5 and 6(f)]. On the other hand,
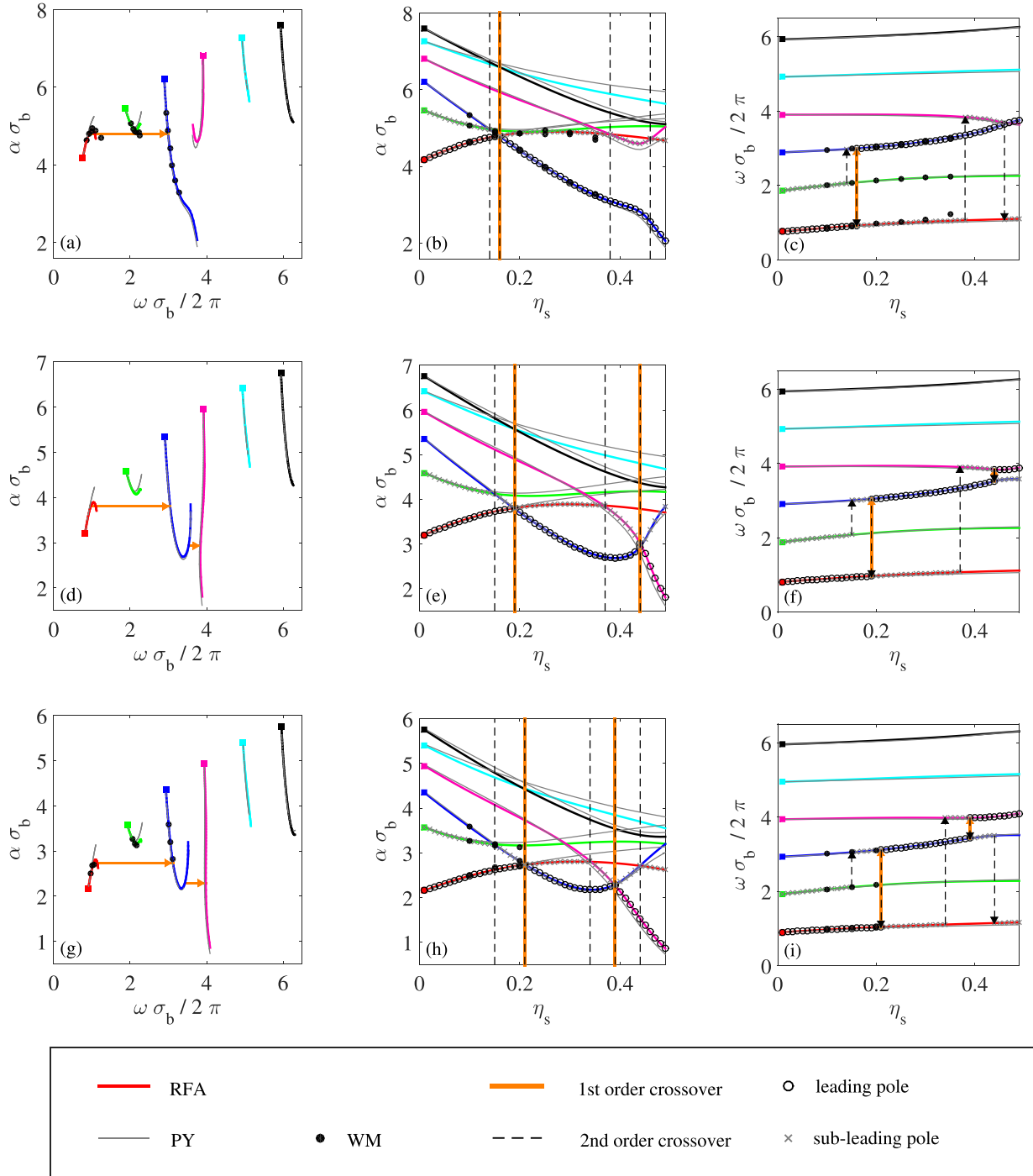
FIG. 7. Dependence of the first six poles on η_s for $q = 0.3$ and $\eta_b = 0.05$ (top panels), $\eta_b = 0.10$ (middle panels), and $\eta_b = 0.20$ (bottom panels). The thick (colored) and thin (gray) lines correspond to the RFA and PY predictions, respectively, while the solid circles represent the WM values for the cases where MD simulations were performed. The colored squares denote poles for a small sphere packing fraction $\eta_s = 0.01$, and the lines indicate trajectories for increasing values of η_s. The horizontal lines denote the crossovers as η_s increases. In the central and right panels, the open circles and crosses represents the leading and subleading poles, respectively.

according to Figs. 9(c), 9(f), and 9(i), a single crossover exists at $\eta_b = 0.20$ and $q = 0.648$ since $\eta_b = 0.05$ and $\eta_b = 0.10$ are located to the right of the end point [see Fig. 3(h)].

Figures 6–9 also show that some quantitative differences between the RFA predictions and those of the PY approximation are present, as already mentioned in connection with Fig. 5. We can observe as well a good agreement of the results

of the RFA method with the poles obtained from the WM scheme for those cases where MD simulations were carried out. This shows (via WM) that the RFA can effectively be used to predict the structural properties of BHS mixtures over a wide range of the phase diagram.

It should be noted that, apart from the damping coefficients and the oscillation frequencies, the amplitudes $A_{ij}^{(n)}$ [see
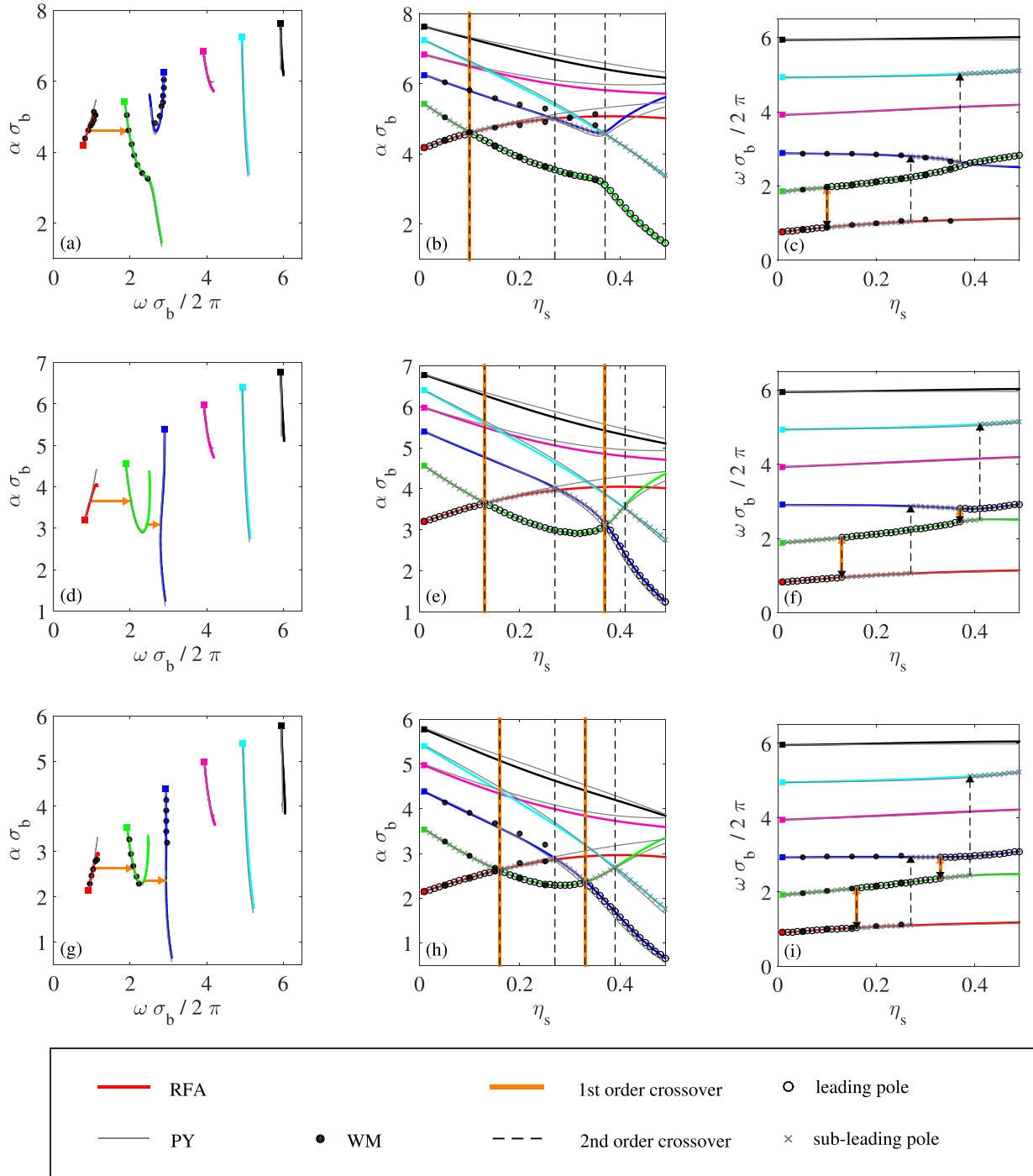
FIG. 8. Same as in Fig. 7, except that in this instance $q = 0.4$.

Eq. (11)] can be obtained from both the RFA and the WM scheme. As an illustration, Fig. 10 shows the η_s-dependence of the amplitudes corresponding to the first three poles in the case $\eta_b = 0.05$ and $q = 0.3$. For this rather disparate mixture, it can be observed that $A_{bb} \sim 10A_{sb} \sim 100A_{ss}$. The general agreement between the RFA and WM results is fair, except for the amplitude A_{bb} associated with the second pole ($\omega\sigma_b/2\pi \equiv \sigma_b/\lambda \approx 2$) when η_s increases. Note, however, that this second pole is never the leading one. If one focuses on the leading and subleading poles ($\sigma_b/\lambda \approx 1$ or $\sigma_b/\lambda \approx 3$), the agreement is very good.

Obviously, this complex behavior concerning the asymptotic decay of $h_{ij}(r)$ and the associated structural crossovers emerge as a consequence of the competition between the three basic length scales of the problem, namely, σ_s, σ_b, and σ_{sb}. Another manifestation of this competition appears when dealing with the sign of the first (local) minimum of $h_{ij}(r)$, here denoted as $h_{ij}^{\min}$, typically located at $r_{ij}^{\min} \approx 2\sigma_{ij}$. The conventional expectation is $h_{ij}^{\min} < 0$, thus signaling the beginning of the oscillations around $h_{ij}(r) = 0$. In fact, this is what happens in monocomponent fluids. However, given η_b and q, it turns out that $h_{ij}^{\min} > 0$ if η_s is smaller than a certain
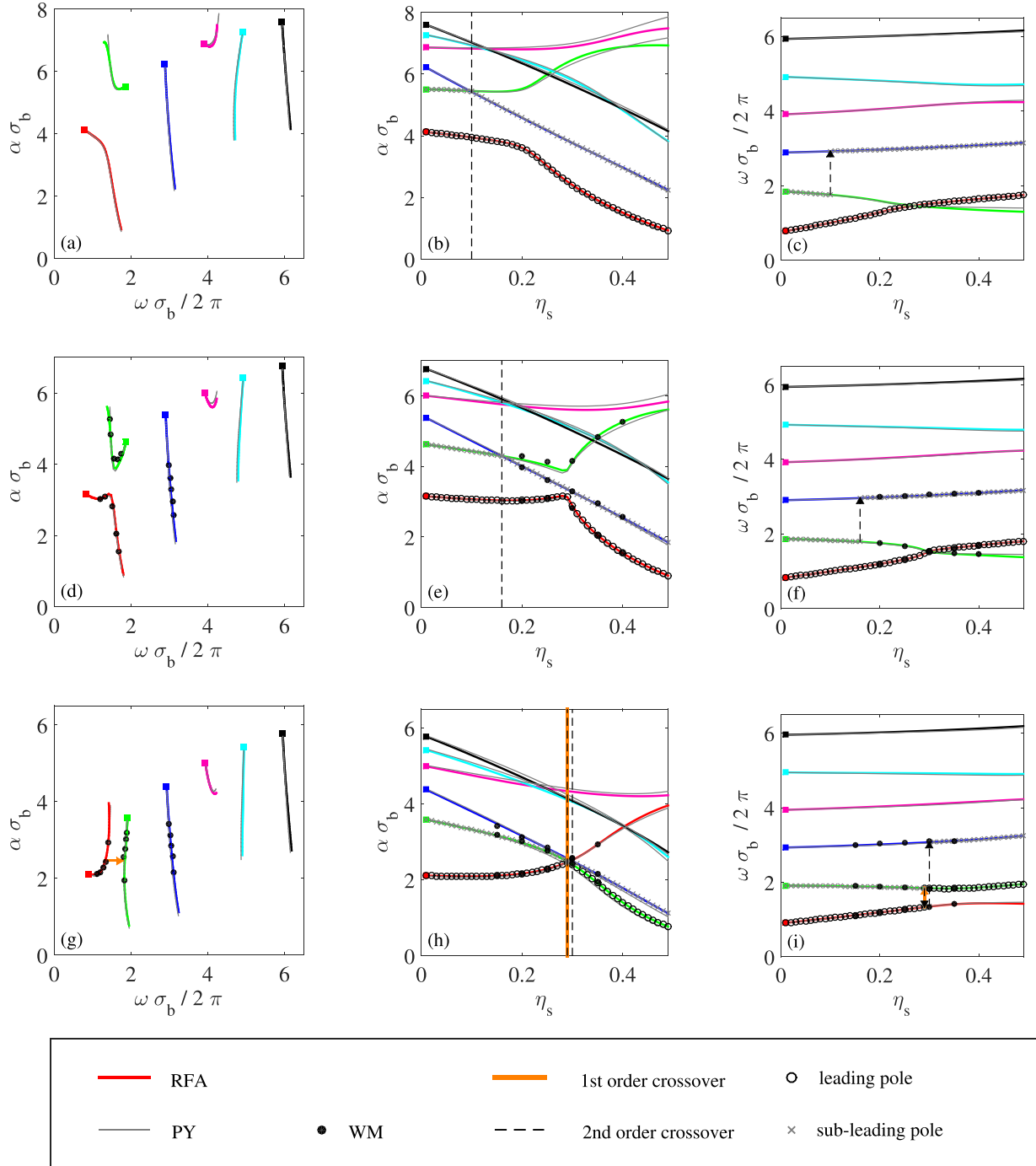
FIG. 9. Same as in Fig. 7, except that $q = 0.648$.

transition value. The loci $h_{ij}^{\min} = 0$ separating the conventional behavior $h_{ij}^{\min} < 0$ (above the locus) from the peculiar property $h_{ij}^{\min} > 0$ (below the locus) are shown in Fig. 11 for $q = 0.2, 0.3,$ and 0.4. Given a value of q, the locus $h_{ss}^{\min} = 0$ envelops the locus $h_{sb}^{\min} = 0$, and the latter envelops the locus $h_{bb}^{\min} = 0$. Additionally, the region with $h_{ij}^{\min} > 0$ shrinks as q increases. Moreover, the curves $h_{sb}^{\min} = 0$ and $h_{bb}^{\min} = 0$ for the cases $q = 0.3$ and 0.4, as well as the curve $h_{ss}^{\min} = 0$ for $q = 0.4$, lose their meaning to the right of the crosses. This is because at a larger value of η_b, $h_{ij}^{\min} = h_{ij}(r \approx 2\sigma_{ij})$ changes

from being a negative local minimum to being negative, but not an extremum, as η_s decreases.

The structural crossover phenomenon is illustrated in Fig. 12, where the decay of $h_{bb}(r)$ at $\eta_b = 0.05$ and (a) $\eta_s = 0.1$ and (b) $\eta_s = 0.3$ for $q = 0.3$ is shown. In agreement with the top rightmost panel of Fig. 7, the leading pole changes from being the first one (wavelength $\lambda \approx \sigma_b$) at $\eta_s = 0.1$ to being the third one (wavelength $\lambda \approx \sigma_s$) at $\eta_s = 0.3$, the transition taking place at $\eta_s \simeq 0.18$. Additionally, Fig. 12(a) shows that, at least for intermediate distances (say, $1 < r/\sigma_b < 2$), the three leading poles are needed

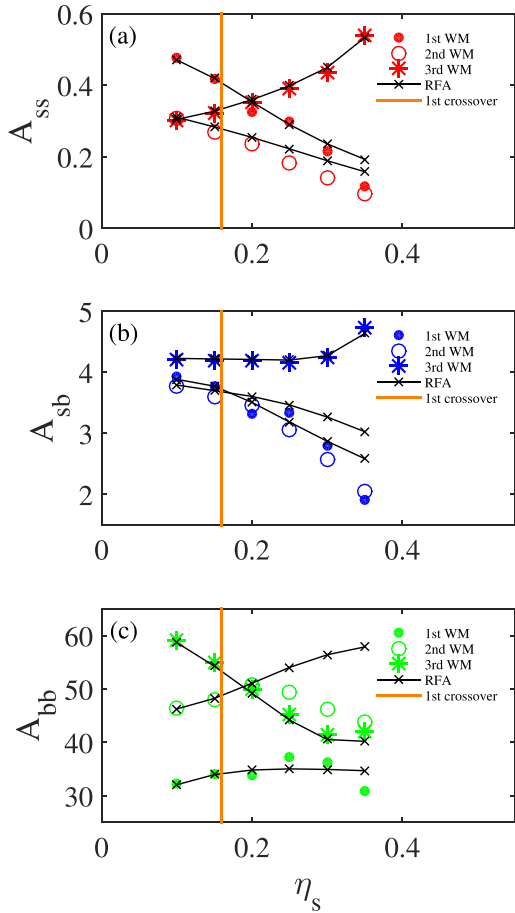FIG. 10. Plot of the amplitudes (a) A_{ss}, (b) A_{sb}, and (c) A_{bb} as functions of η_s at $\eta_b = 0.05$ for $q = 0.3$. The first three poles (in order of increasing ω) are considered. The vertical thick (orange) line at $\eta_s \simeq 0.16$ represents a structural crossover.

to capture the (large-wavelength) oscillations of $h_{bb}(r)$ at $\eta_s = 0.1$. This situation becomes even more relevant as one approaches the transition value $\eta_s \simeq 0.18$ since the damping coefficients associated with the three first poles almost coincide near $\eta_s \simeq 0.18$ [see Fig. 7(b)]. However, at $\eta_s = 0.3$, Fig. 12(b) shows that the leading pole is enough to account for the (small-wavelength) oscillations, even for intermediate distances.

V. CONCLUDING REMARKS

The results we have presented in this paper deserve more consideration. First of all, it must be emphasized that the good agreement found between the results of the RFA method and those of the WM scheme in paper I [12] for a single value of the total packing fraction ($\eta = 0.5$) and size ratio ($q = 0.648$) has been hereby confirmed. Therefore, we now have a powerful theoretical (almost completely analytic) tool to examine the complex behavior of the structural properties of BHS mixtures, including their asymptotic decay. In particular, we have found that, in the case of the leading pole of the total correlation functions, given a value of η_s, the (reduced) damping coefficient $\alpha\sigma_b$ generally decreases with increasing η_b, while it exhibits a nonmonotonic dependence on η_s at fixed
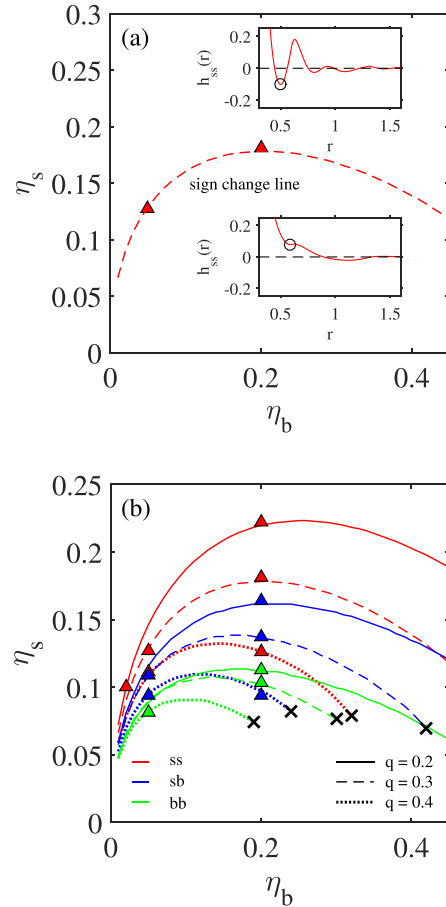

FIG. 11. (a) Locus $h_{ss}^{\min} = 0$ [i.e., line of changing sign in the value of the first minimum of $h_{ss}(r)$], as predicted by the RFA, for a size ratio $q = 0.3$. The insets show representative behaviors of $h_{ss}(r)$ above and below the locus, and the triangles are MD results. (b) RFA predictions for the loci (from top to bottom for each q) $h_{ss}^{\min} = 0$ (red), $h_{sb}^{\min} = 0$ (blue), and $h_{bb}^{\min} = 0$ (green). The size ratios are $q = 0.2$ (solid lines), $q = 0.3$ (dashed lines), and $q = 0.4$ (dotted lines). In each case, $h_{ij}^{\min} > 0$ in the region below the corresponding curve. Some of the curves end at the points marked with crosses. The triangles represent MD results.

η_b. Also, the influence of q on $\alpha\sigma_b$ appears to be rather weak, although there is a general tendency for a slight decrease with increasing q at fixed (η_b, η_s).

On the other hand, in agreement with the work of Grodon *et al.* [27,29] (which considered a different approximation and a particular value of q), we have confirmed that there exists a crossover line (C) in the plane η_s vs η_b separating a region (R_1) where the (reduced) natural oscillation frequency $\omega\sigma_b/2\pi \equiv \sigma_b/\lambda$ is of the order of 1 from another region (R_{n_s}, with $n_s \approx 1/q$) where σ_b/λ is of the order of $1/q$. The former extends to smaller values of η_s, while the latter extends to larger values of η_s. Further, we have also found that, if q is small enough, there is a second crossover line (C') separating R_{n_s} from a third region (R_{n_s+1}) where σ_b/λ is of the order of the first harmonic of $\sigma_b/\lambda = 1$ that turns out to be larger than n_s. This line C' may terminate at an end point located at a large value of η_s and a small value of η_b, which implies that one can move continuously between regions R_{n_s} and R_{n_s+1} by circumventing the end point from the left. However, except for
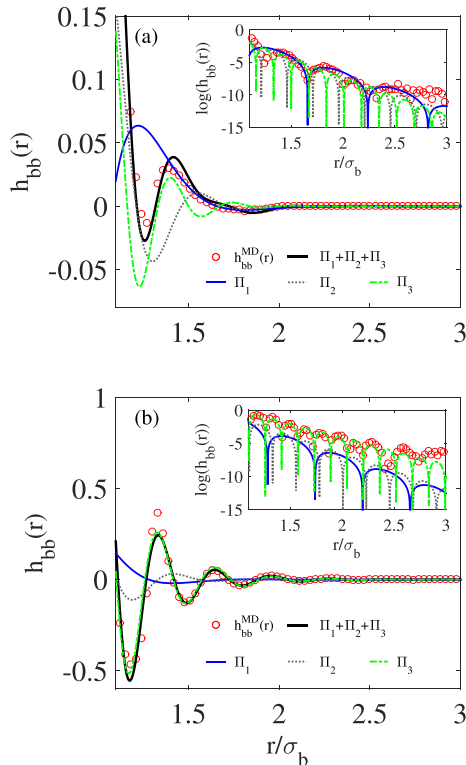
FIG. 12. Big-big correlation function $h_{bb}(r)$ for $q = 0.3$, $\eta_b = 0.05$, and (a) $\eta_s = 0.1$, (b) $\eta_s = 0.3$. The (red) open circles are MD data, while the (blue) solid, (gray) dotted, and (green) dashed lines represent the contribution of the first (Π_1), second (Π_2), and third (Π_3) pole, respectively. Note that at $\eta_s = 0.1$ the leading pole describing the asymptotic decay of $h_{bb}(r)$ is Π_1 and at $\eta_s = 0.3$ it is Π_3.

small q, this line tends to lie above the region $\eta_s + \eta_b = 0.5$, where the fluid phase is expected to coexist with the solid

one. Finally, we have also shown that the above scenario can even be more complex, with additional crossover lines (C' separating R_{n_s} from R_{n_s-1} and C'' separating R_1 from R_{n_s-1}) and splitting points, as the total packing fraction $\eta = \eta_s + \eta_b$ increases or the size ratio q decreases. One important issue, which remains to be assessed, is to understand the behavior of the crossover lines in the limiting region $\eta_b \rightarrow 0$. It should be remarked that this region is hardly accessible by simulations but certainly needs to be studied in more depth.

To close this paper, two other outcomes of our work are worth pointing out. The first one concerns the value of the first local minimum in the total correlation function $h_{ij}(r)$, which changes sign as one crosses a certain transition line which depends on q and the pair under consideration. This point is dealt with by Fig. 11. The second is that the direct correlation function $c_{sb}(r)$ is not monotonic in the region $0 < r < \sigma_{sb}$ and presents a well-defined minimum. To our knowledge, this feature has not been pointed out before. Due to the fact that we are persuaded that this finding is relevant, we will address this point and analyze it in detail in the following (third) paper of this series.

[1] J. A. Barker and D. Henderson, What is "liquid"? Understanding the states of matter, Rev. Mod. Phys. **48**, 587 (1976).

[2] J.-P. Hansen and I. R. McDonald, *Theory of Simple Liquids*, 4th ed. (Academic Press, London, 2013).

[3] A. Santos, *A Concise Course on the Theory of Classical Liquids. Basics and Selected Topics*, Lecture Notes in Physics, Vol. 923 (Springer, New York, 2016).

[4] M. E. Fisher and B. Widom, Decay of correlations in linear systems, J. Chem. Phys. **50**, 3756 (1969).

[5] R. Evans, J. R. Henderson, D. C. Hoyle, A. O. Parry, and Z. A. Sabeur, Asymptotic decay of liquid structure: Oscillatory liquid-vapour density profiles and the Fisher–Widom line, Mol. Phys. **80**, 755 (1993).

[6] C. Vega, L. F. Rull, and S. Lago, Location of the Fisher-Widom line for systems interacting through short-ranged potentials, Phys. Rev. E **51**, 3146 (1995).

[7] W. E. Brown, The Fisher–Widom line for a hard core attractive Yukawa fluid, Mol. Phys. **88**, 579 (1996).

[8] M. Dijkstra and R. Evans, A simulation study of the decay of the pair correlation function in simple fluids, J. Chem. Phys. **112**, 1449 (2000).

[9] P. Tarazona, E. Chacón, and E. Velasco, The Fisher–Widom line for systems with low melting temperature, Mol. Phys. **101**, 1595 (2003).

[10] T. Škrbić, A. Badasyan, T. X. Hoang, R. Podgornik, and A. Giacometti, From polymers to proteins: The effect of side chains and broken symmetry on the formation of secondary structures within a Wang–Landau approach, Soft Matter **12**, 4783 (2016).

[11] M. López de Haro, A. Rodríguez-Rivas, S. B. Yuste, and A. Santos, Structural properties of the Jagla fluid, Phys. Rev. E **98**, 012138 (2018).

[12] S. Pieprzyk, A. C. Brańka, S. B. Yuste, A. Santos, and M. López de Haro, Structural properties of additive binary hard-sphere mixtures, Phys. Rev. E **101**, 012117 (2020).

[13] A. Statt, R. Pinchaipat, F. Turci, R. Evans, and C. P. Royall, Direct observation in 3d of structural crossover in binary hard sphere mixtures, J. Chem. Phys. **144**, 144506 (2016).

[14] S. B. Yuste, A. Santos, and M. López de Haro, Structure of multicomponent hard-sphere mixtures, J. Chem. Phys. **108**, 3683 (1998).

[15] M. López de Haro, S. B. Yuste, and A. Santos, Alternative approaches to the equilibrium properties of hard-sphere liquids,

in *Theory and Simulation of Hard-Sphere Fluids and Related Systems*, Lecture Notes in Physics, Vol. 753, edited by A. Mulero (Springer, Berlin, 2008), pp. 183–245.

[16] A. Santos, S. B. Yuste, and M. López de Haro, Structural and thermodynamic properties of hard-sphere fluids, J. Chem. Phys. **153**, 120901 (2020).

[17] J. L. Lebowitz, Exact solution of generalized Percus–Yevick equation for a mixture of hard spheres, Phys. Rev. **133**, A895 (1964).

[18] T. Boublík, Hard-sphere equation of state, J. Chem. Phys. **53**, 471 (1970).

[19] E. W. Grundke and D. Henderson, Distribution functions of multi-component fluid mixtures of hard spheres, Mol. Phys. **24**, 269 (1972).

[20] L. L. Lee and D. Levesque, Perturbation theory for mixtures of simple liquids, Mol. Phys. **26**, 1351 (1973).

[21] A code using the Mathematica computer algebra system to obtain $G_{ij}(z)$ and $g_{ij}(r)$ with the RFA method is available from the web page http://www.unex.es/eweb/fisteor/santos/filesRFA.html.

[22] M. N. Bannerman, R. Sargant, and L. Lue, DynamO: a free $\mathcal{O}(n)$ general event-driven molecular dynamics simulator, J. Comput. Chem. **32**, 3329 (2011).

[23] M. P. Allen and D. J. Tildesley, *Computer Simulation of Liquids* (Oxford University Press, Oxford, 2017).

[24] J. J. Salacuse, A. R. Denton, and P. A. Egelstaff, Finite-size effects in molecular dynamics simulations: Static structure factor and compressibility. I. Theoretical method, Phys. Rev. E **53**, 2382 (1996).

[25] A. Baumketner and Y. Hiwatari, Finite-size dependence of the bridge function extracted from molecular dynamics simulations, Phys. Rev. E **63**, 061201 (2001).

[26] R. Evans, R. J. F. Leote de Carvalho, J. R. Henderson, and D. C. Hoyle, Asymptotic decay of correlations in liquids and their mixtures, J. Chem. Phys. **100**, 591 (1994).

[27] C. Grodon, M. Dijkstra, R. Evans, and R. Roth, Decay of correlation functions in hard-sphere mixtures: Structural crossover, J. Chem. Phys. **121**, 7869 (2004).

[28] S. Pieprzyk, A. C. Brańka, and D. M. Heyes, Representation of the direct correlation function of the hard-sphere fluid, Phys. Rev. E **95**, 062104 (2017).

[29] C. Grodon, M. Dijkstra, R. Evans, and R. Roth, Homogeneous and inhomogeneous hard-sphere mixtures: manifestations of structural crossover, Mol. Phys. **103**, 3009 (2005).

[30] J. Baumgartl, R. P. A. Dullens, M. Dijkstra, R. Roth, and C. Bechinger, Phase diagram of highly asymmetric binary hard-sphere mixtures, Phys. Rev. Lett. **98**, 198303 (2007).

[31] See file movie.mp4 in the Supplemental Material at http://link.aps.org/supplemental/10.1103/PhysRevE.104.024128 for a video with the evolution of $\omega\sigma_b/2\pi$ in the plane η_s vs η_b from $q = 0.65$ to $q = 0.2$.

[32] M. Dijkstra, R. van Roij, and R. Evans, Phase diagram of highly asymmetric binary hard-sphere mixtures, Phys. Rev. E **59**, 5744 (1999).